J. Fluid Mech. (2008), *vol.* 616, *pp.* 31–41.
doi:10.1017/S0022112008003819 Printed in the United Kingdom

Experiments on standing bubbles in a vertical pipe

GENNARO DELLO IOIO AND ANDREW W. WOODS

BP Institute, University of Cambridge, Cambridge, CB3 0EZ, UK

(Received 11 December 2007 and in revised form 12 August 2008)

We present a series of laboratory experiments in which a steady stream of air is supplied through a small hole in the wall of a vertical pipe of rectangular cross-section down which there is a steady flux of water. For a range of liquid flow rates, the air forms a steady standing bubble whose nose is attached to the point of air supply. The steady bubble sheds a flux of much smaller air bubbles at its base, located downstream of the air injection point. The minimum liquid speed for which steady standing bubbles develop occurs at a particular Froude number of the liquid flow, $Fr_d = U/\sqrt{gd} = 0.38$, where U is the upstream speed, g the acceleration due to gravity and d the width of the cell. These trapped bubbles are distinct from the freely rising Taylor bubble, in that the Froude number at the nose is variable. Also, on a length scale greater than that influenced by surface tension, we find that the bubble nose asymptotes to a cusp-like shape, with an angle that decreases with Fr_d. We show that numerical solutions of the potential flow equations replicate the bubble shape and angle of the cusp, which appear independent of the gas flux. We also find that there is a minimum gas flux for which these standing bubbles develop. As the gas flux decreases below this threshold, the standing bubbles become unstable and, instead, a much shorter oscillating bubble develops. This produces a wake which has similarities with that formed downstream of a cylinder in a confined channel, but which also carries bubbles downstream. We also find that with sufficiently small gas flux, no bubble develops. For liquid flow rates smaller than the critical value, $Fr_d < 0.38$, we find that the bubbles become unstable and detach from the injection point and rise up the tube.

1. Introduction

For the past 60 years there has been a continued interest in the dynamics of free bubbles rising in a vertical tube, owing to their importance in a wide range of applications. The initial pioneering works of Dumitrescu (1943) and Davies & Taylor (1950) analysed the rise speed of the bubbles in a circular pipe, using potential theory, and established that the rise speed U varies as a function of the pipe radius according to the relation

$$U \approx 0.5\sqrt{gR} \tag{1}$$

where R is the pipe radius and g is the gravitational acceleration. Numerous subsequent papers have attempted to describe the shape of the freely rising bubble near the nose (Batchelor 1967; Collins *et al.* 1978). Recently Clanet, Héraud & Searby (2004) generalized the model of Dumitrescu, to describe the rise speed of free bubbles

in pipes of different cross-sectional geometry, and proposed the relation

$$U \approx 0.2\sqrt{gP} \tag{2}$$

where P is the wetted perimeter of the tube.

Following a different approach, Keller & Geer (1973) and then Vanden-Broeck (1984*a*), used potential theory to examine the shape of a theoretical, long bubble rising with a prescribed speed through a two-dimensional tube. For ease of calculation, the model was developed in the frame of the bubble, with an upstream flow equal to the bubble rise speed, and the shape of the bubble was analysed as a function of the Froude number

$$Fr_d = \frac{U}{\sqrt{gd}} \tag{3}$$

where d is the width of the tube and g the acceleration due to gravity. This analysis identified that, in the absence of surface tension, there is a critical Froude number, $Fr_d = 0.36$, for the bubble at which the nose ceases to be horizontal. For larger Froude numbers, the theoretical bubble shape develops a cusp which subtends zero angle at its nose. Downstream of the nose the bubble rapidly approaches the theoretical shape predicted by slender jet theory, in which the interior pressure of the bubble is a constant and the liquid flow is essentially parallel to the walls of the tube. Further modelling by Vanden-Broeck (1984*b*) identified that surface tension leads to the formation of cusped bubbles of finite angle, such that the angle at the cusp decreases with Froude number, although he states that these solutions are not physical at the cusp; instead, one expects a localized region of high curvature at the nose connecting each side of the bubble. In a different model, Vanden-Broeck (1984*c*) has indeed shown that if there is an elliptical object of small thickness at the tip of the bubble, then each side of the bubble may separate from this object with finite angle to the direction of the upstream flow.

Although of theoretical interest, it is not clear that such mathematical solutions for a standing bubble may arise in practice. Indeed, the majority of experimental observations of freely rising bubbles are in accord with the results of Dumitrescu and Taylor, and suggest that the bubble rises with a particular (natural) Froude number (equations (1) and (2)) and that the nose of the bubble is smooth on a scale much larger than the capillary scale.

However, it may be possible for forced, standing bubbles to develop if there is a steady downward flow of liquid in a tube in which a continuous source of gas is supplied through the wall at a fixed point. If the liquid flow rate exceeds a critical Froude number, then one might expect that a trapped bubble can form downstream of the injection point, and that its shape would be determined to good approximation by potential theory.

We now report on a series of experiments for this flow configuration, and identify a range of Froude numbers for which such 'forced' trapped bubbles do indeed develop. We also show that within the resolution of our experiments, the bubbles develop a cusp-like structure near the nose, with an angle which is consistent with some new numerical predictions from potential theory in the limit of small surface tension. The shapes are cusp-like, in that outside a very small region of high curvature, < 1 mm, at the nose, the bubble appears to subtend a finite angle with the vertical. The experiments also reveal that the stability and downstream extent of these bubbles is strongly dependent on the gas flux supplied to its nose. For small gas fluxes, the long quasi-steady bubbles become unstable, and a much shorter, oscillating bubble

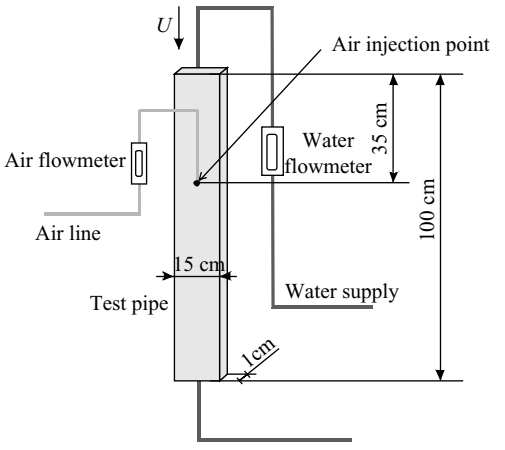

FIGURE 1. Schematic of the experimental apparatus.

develops, again anchored at the point of gas injection. These oscillating bubbles shed vortices and small bubbles which are swept downstream in a wake somewhat analogous to that formed downstream of an obstacle in a uniform flow (Roshko 1954; Deniz & Staubl 1997).

As well as being of fundamental interest, recognition of such forced, trapped bubbles is important for two-phase pipe flow in which liquids may enter through perforated walls of the pipe. For example, during the production of oil, well bores are often inclined to the horizontal, and if any gas breaks through into the well, one can envisage situations in which liquid–gas counterflow develops (Dake 1979). Formation of a long, trapped bubble downstream of the gas inflow point may cause pressure losses and hence compromise production from upstream.

It may also be of interest to note that, although the physical systems are different, some of the bubble shapes are reminiscent of pre-mixed turbulent V-flames which develop downstream of a flameholder in a free stream (Rhee, Talbot & Sethian 1995).

2. Experimental study

Figure 1 illustrates the apparatus used in the series of experiments reported in this paper. There is a vertical pipe 1.0 m in length of rectangular cross-section, 15 cm × 1 cm, at the top of which a steady stream of water is supplied; 35 cm below the top of the tube there is a hole of diameter 1 mm in the centre of one of the wider sides. An air line, connected to a compressor, supplies a constant flux of air to this opening. The liquid flow thus travels over 18 hydraulic diameters prior to reaching the gas inflow port, and therefore has become fully turbulent. The flow rate of both air and water was measured through rotating flowmeters (Key Instruments MR3A02 for the air, Krohne VA20 for the water). The experiments were recorded using digital video and digital photography using a Nikon 995 camera; a 1 kW uniform backlight was used to illuminate the flow. The remainder of the laboratory was blacked out to improve contrast.

The range of liquid flow rates used in the experiments, 400–2500 $\mathrm{cm^3\,s^{-1}}$, imply Reynolds numbers, $Re = U R_H/\nu$, of order 10 000–35 000, where R_H is the hydraulic radius of the cell, defined as $2A/P$ where A is the cross-sectional area and P the perimeter of the cell, and ν the kinematic viscosity, and hence we expect the effects of

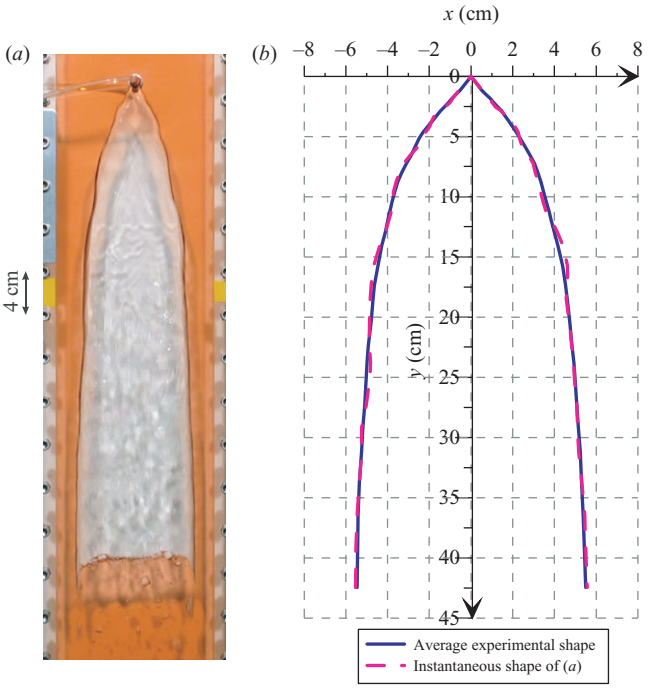

FIGURE 2. (*a*) Photograph showing a typical quasi-steady bubble. (*b*) The averaged profile, computed from the average of 20 frames, lies within about 5 mm of each instantaneous shape of the bubble. Note the horizontal and vertical axes have different scales in (*b*). The experiment shown in (*a*) has $Q_w = 1.1\ \mathrm{l\,s^{-1}}$ ($Fr_d = 0.60$) and $Q_g = 2.0\ \mathrm{l\,min^{-1}}$ ($G = 0.018$).

viscous resistance from the wall to be small. On the scale of the cell width, the effects of surface tension are of secondary importance compared to the buoyancy forces as may be seen from the relatively large Bond number $Bo = \rho g R_H^2/\sigma \approx 11$, where σ is the surface tension and ρ is the density (Clanet *et al.* 2004). Indeed, with a flow of speed $1\ \mathrm{m\,s^{-1}}$ near the tip of the bubble, the surface tension σ/r associated with an interface of curvature r becomes comparable to the fluid inertia ρu^2 only with interface curvature of order $r \sim 10^{-4}$ m. This suggests that surface tension has only a secondary effect except in a localized zone at the tip of the bubble, of scale smaller than or comparable to the gas inflow opening, which has diameter 0.001 m.

In a typical experiment, as the water flux was increased for a fixed gas flux, it reached a critical value at which the downflowing water swept the gas downstream. For sufficiently large gas flux, a standing gas bubble then formed immediately below the gas injection site. These bubbles appeared to be two-dimensional features, and extended up to 50 cm downstream of the injection point. The downstream tail of the bubbles extended up to 10–12 cm across the width of the tube. The tail of the bubble has a somewhat flat surface, and there is a region of recirculation in the wake directly behind the bubble, with a rapid jet-like flow of liquid continuing downwards on each side of this wake. The wake flow is reminiscent of the turbulent wake directly behind a spherical cap bubble (Wegener & Parlange 1973). At the downstream edge of the bubble, a series of very small gas bubbles, of size 2–3 mm, continually peeled off and were carried downstream in this jet. Figure 2(*a*) is a photograph which illustrates the shape of a typical quasi-steady gas bubble. Small perturbations may be seen on

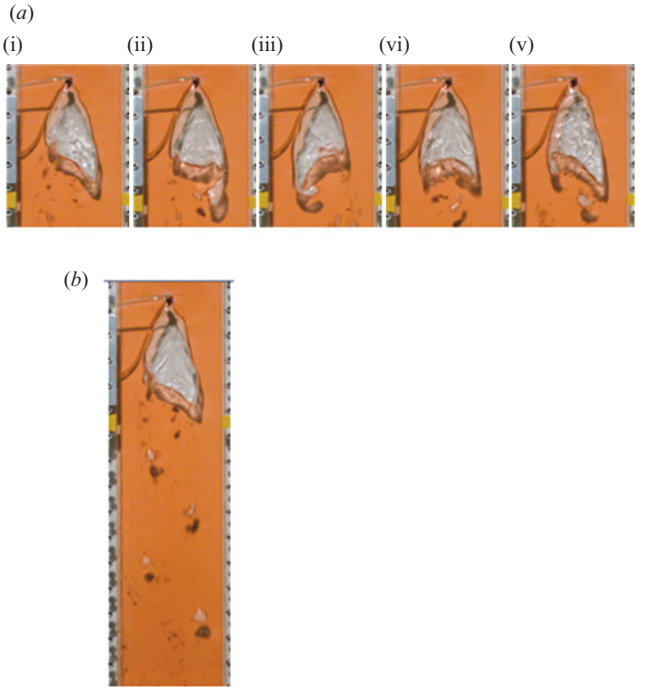

FIGURE 3. (*a*) Photographs illustrating the shape of the oscillatory bubble at five different points in the cycle, (i) to (v). This indicates the periodic asymmetrical shedding of bubbles as each side of the tail becomes extended and breaks off to be swept downstream. The bubble shown in the figure has been obtained with a water flux $Q_w = 0.95\,\mathrm{l\,s^{-1}}$ ($Fr_d = 0.52$) and an air flux $Q_g = 1.0\,\mathrm{l\,min^{-1}}$ ($G = 0.08$) and oscillates at a frequency of 3.3 Hz. (*b*) Photograph of the wake downstream of the bubble.

the surface of the bubble; these are advected downstream, and appear to decay with distance. Figure 2(*b*) illustrates the average of 20 photographs of the shape of the gas bubble. This average lies within about 5 mm of each of the instantaneous bubble shapes, confirming that the bubble is stable, and that the perturbations to the bubble surface do not grow as they move downstream. As an example, this average shape may be compared with the dashed line in figure 2(*b*), which is a trace of the bubble in figure 2(*a*).

As the gas flux was decreased, a critical value was reached at which these long steady bubbles were no longer stable, and there was a transition to a much shorter bubble which executed large-amplitude oscillations just downstream of the injection port, to which it was anchored. The pattern of flow observed for these oscillatory bubbles is shown in figure 3(*a*). During each oscillation, the tail of the bubble extends downstream first on one side and then on the other side of the channel. As the tail passes through the point of maximum displacement of the oscillation, the tail separates and is swept downstream. Following each separation event, an eddy also propagates downstream. This leads to a downstream wake which is somewhat analogous to a vortex street, but which also carries discrete bubbles (figure 3*b*).

For the range of gas fluxes for which either the steady long bubbles or the short oscillatory bubbles developed, then, for a given liquid flux, the shape of the bubble near the nose appears to be independent of the gas flux. In the next section we show

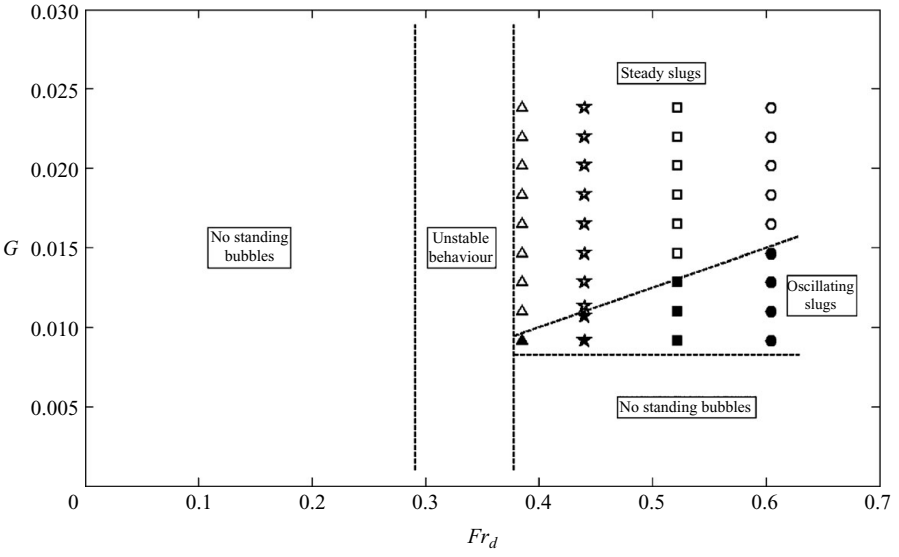

FIGURE 4. Regime diagram illustrating the transitions between the long quasi-steady and short oscillating bubbles as a function of the Froude number (x-axis) and the dimensionless gas flux G (y-axis); it can been seen that no stable standing bubble develops for $Fr_d < 0.38$. Solid symbols represent oscillating slugs while open symbols represent steady slugs; triangles, stars, squares and circles represent Froude numbers $Fr_d = 0.38$, 0.44, 0.52 and 0.60.

some numerical solutions from steady potential theory which replicate the shape of both the time-averaged quasi-steady long bubbles (figure 2*b*) and the near-nose part of the shorter oscillatory bubbles (figure 3*a*).

We have built a regime diagram, based on our observations that the stability of the long standing bubbles varies as a function of the liquid flux, Q_w, and the gas flux, Q_g. This is shown figure 4, which illustrates the flow regime as a function of (*a*) the upstream Froude number, $Fr_d = U/\sqrt{gd}$, which is equivalent to the dimensionless liquid flux, $Q_w/(A\sqrt{gd})$, since $Q_w = AU$, and (*b*) the dimensionless gas flux, $G = Q_g/(A\sqrt{gd})$, where A is the cross-sectional area of the cell. It is seen that for liquid Froude numbers smaller than the critical value $Fr_d = 0.38$ the standing slugs are unstable, and for $Fr_d < 0.3$ no standing bubble appears. Instead, for the experimental conditions examined herein, the air either rises from the injection point or is swept downstream in small bubbles. For larger liquid Froude numbers, $Fr_d > 0.38$ the figure shows that as the gas flux decreases there is a transition from the long steady to the short oscillatory bubbles as described above.

The flow associated with the oscillatory bubbles is somewhat analogous to observations of vortex shedding from fixed and oscillating obstacles in a confined channel (Roshko 1954; Deniz & Staubl 1997; Carberry, Sheridan & Rockwell 2005). There is a wide literature of such experiments conducted at Reynolds numbers comparable to those in the present experiments, and it has been observed that the frequency of vortex shedding, f, when expressed in dimensionless form $St = fa/U$, where U is the mean speed and a the width of the obstacle, has value of order 0.1–0.3. Also, St has been observed to increase as the ratio of width of the obstacle a to the width of the channel, d, increases (Richter & Naudascher 1976) and Hiwada & Mabuchi (1981) found that with a sufficiently wide obstacle relative to channel width, $a/d > 0.6$, the vortex shedding ceased. Our experiments show similar features to

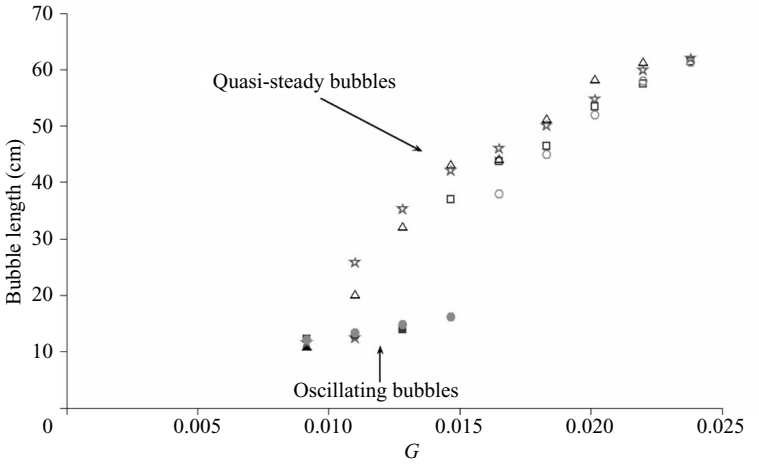

FIGURE 5. Length of bubbles as a function of the air flux, expressed in dimensionless form G. Triangles, stars, squares and circles represent, respectively, water Froude numbers of 0.38, 0.44, 0.52, 0.60.

these experimental observations. For example, for the bubble shown in figure 3, the frequency of oscillation is 3.3 Hz corresponding to $St \sim 0.3$. Also, for our experiments, the transition from the oscillating bubble to the longer steady bubble occurs when the bubble width reaches a fraction of order 0.5–0.6 of the width of the pipe.

Some insight into the transition from the oscillatory bubble regime to the long steady bubble regime emerges from the observation that for small gas fluxes, the periodic shedding of discrete bubbles and their transport in the wake (figure 3*b*) carries all the gas injected into the flow downstream. If u is the downstream flow speed in the wake, and u_b is the average rise speed of these discrete bubbles relative to the liquid, then the flux may also be written as $\phi dw(u - u_b)$ where ϕ is the void fraction of bubbles in the wake, and dw is the cross-sectional area of the experimental flow pipe. Therefore, as the gas flux increases, the void fraction ϕ also increases. Eventually, with sufficient gas flux, this leads to bubble mergers and a further increase in void fraction in the wake as the rise speed of the merged bubbles increases.

As a result, the wake is unable to transport the gas downstream, and the main bubble becomes progressively longer until reaching a new quasi-steady shape. A very fast liquid flow then develops on each side of the bubble and this removes a large flux of small bubbles from the downstream edge of the main bubble, leading to a different mechanism for the gas transport. This phenomenological picture of the transition from oscillatory to steady bubbles, based on the ability of the wake to transport the gas as discrete bubbles, is also consistent with experimental data which show that the maximum gas flux for which the oscillatory bubbles form, increases with the liquid flow rate.

We find that the length of the steady bubbles increases with gas flux, but decreases with liquid flux (figure 5). This observation may be rationalized by noting that, with the long standing bubble, the erosion of small bubbles from the downstream outer edge of the bubble supplies the gas flux, which is carried by the jet-like flow of liquid near the wall, downstream of the bubble. As the bubble length increases, the near-wall liquid flow speed also increases (see § 3); in turn, with a higher liquid flow speed, the near-wall jet is able to erode a greater flux of small bubbles from the downstream

edge of the bubble. Hence a larger gas flux or smaller liquid flux will tend to increase the bubble length.

As the upstream Froude number decreases below 0.38, the bubble becomes progressively more unstable and undergoes a series of large-amplitude fluctuations in shape and position as it attempts to rise from the point source, and is then swept downwards by the flow. With $Fr_d < 0.3$ air bubbles were observed to rise immediately from the injection point through the descending liquid stream. It is interesting to note that the results of Clanet *et al.* (2004) for the rise speed of a free bubble in a rectangular pipe may, in the present case, be expressed as $Fr_d = 0.3$ which is consistent with these observations. It is relevant to note that our experiments have been limited to a cell of width 15 cm (figure 1), and we have not studied the behaviour of the injected gas stream in a cell of much larger width, for which the Froude number may fall below 0.2 and different flow regimes may exist.

3. Potential theory description of steady bubbles

In the limit that the pressure variation in the bubble is small relative to that of the liquid, its average shape can be approximated by applying two-dimensional potential theory to model the liquid flow past a surface of constant pressure with zero surface tension. We have developed a finite element numerical model to solve the potential flow in the liquid zone using the Galerkin method as described in Rao (1999). We assume an initial arbitrary shape for the bubble, using a polyline, and then solve for the flow around it considering it as a rigid surface. We then examine the variation of the pressure along the surface of the bubble, and adjust the location of the surface iteratively, in an attempt to generate a surface of uniform pressure. We compare the shape of the calculated bubbles when the pressure fluctuations along the surface of the bubble are smaller than different thresholds to calculate the steady-state shape of the bubble. These numerical solutions suggest that the bubble asymptotes to a cusp-like shape at the nose, and the angle subtended by this cusp with the vertical decreases with the Froude number (e.g. figures 6, 7). The angle is determined by fitting each side of the bubble with a polynomial, and calculating the gradient at the nose; we checked convergence of the numerical solutions by changing the size of the numerical mesh for a given Froude number, and ensuring this angle was invariant. We note that in practice, we expect that at the nose there will be a region of high curvature (of dimension 10^{-3}–10^{-4} m in our experiments), in which the surface tension balances the inertia. This region connects each side of the bubble, so that strictly there is no cusp, although our numerical calculations do not include surface tension and so cannot resolve this.

Figure 6 compares the shapes of the bubbles which we have generated numerically with the shapes of the experimental bubbles for three different flow rates. It is seen that the numerical solutions are in very close agreement with the experimental observations in terms of the shape of the bubble. In figure 7, we show the angle of the apparent cusp at the nose of the experimental bubbles, as estimated by a curve fit through the averaged bubble shape, and this is compared with the predictions of the numerics. As for the bubble shape, there is very good agreement between the numerical solutions and the experimental observations.

Our numerical solutions also coincide with the theoretical bubble shapes published by Vanden-Broeck (1984*a*), up to the resolution of the thickness of the lines in his figure; however, the cusp of zero angle which he predicts theoretically is unphysical owing to the finite surface tension. In a later paper (Vanden-Broeck 1984*b*) he shows

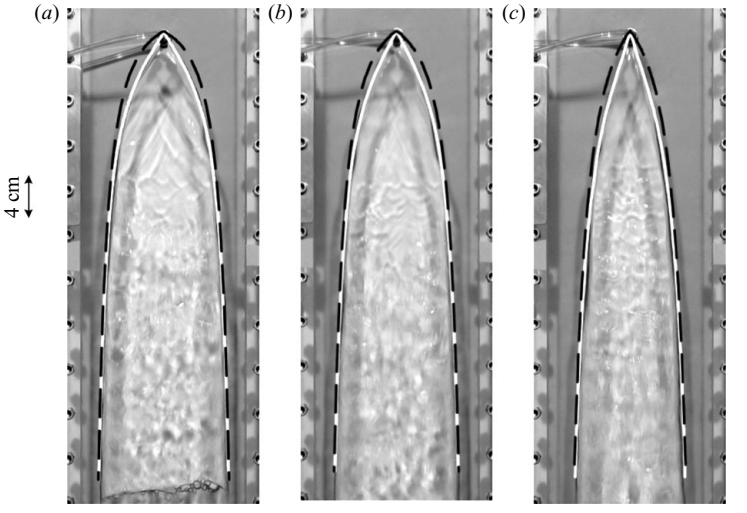

FIGURE 6. Comparison between experimental and numerical (solid line) bubble shapes for three values of the Froude number (*a*) $Fr_d = 0.38$, (*b*) $Fr_d = 0.44$, (*c*) $Fr_d = 0.52$. The dashed line represents the prediction from slender jet theory (4).

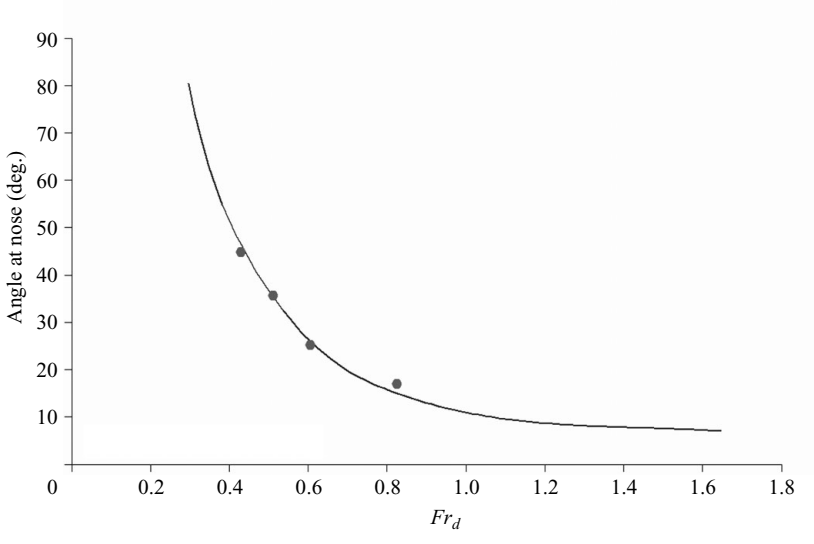

FIGURE 7. Angle which the flow subtends at the nose of the bubble as a function of the Froude number, as determined from the numerical solution (solid line) and the experiments (symbols).

that with finite surface tension the angle of the cusp varies with Froude number, and, although noting that the cusp is unphysical, in a further paper (Vanden-Broeck 1984*c*) he shows that if there is a thin smooth plate present at the nose, then the flow on each side of the plate subtends a finite angle with the plate. This is consistent with the present picture, except that here it seems to be the bubble itself which has a narrow region of high curvature at the nose connecting each side of the bubble. The agreement between our numerical bubble shapes and Vanden-Broeck's (1984*a*) predictions away from the immediate vicinity of the nose, in the limit of high Weber

number, suggests that the detail of the flow at the nose does not control the shape far downstream, beyond the region in which surface tension is important.

In figure 6, for completeness, we also compare the numerical bubble shape with the prediction from the slender jet model (Keller & Geer 1973). This model assumes that the liquid flow is parallel to the walls of the tube, and combining this with the constant pressure of the bubble and Bernoulli's principle, leads to the prediction (cf. Vanden-Broeck 1984*a*)

$$y = \frac{dFr_d^2}{2}\left(\frac{1}{(1-2|x|/d)^2} - 1\right) \tag{4}$$

where y is the distance downstream, such that $y = 0$ when $x = 0$ (figure 2*b*). It is seen that, although the slender jet model is unable to describe the shape near the nose of the bubble, it does provide a good representation of the bubble shape further downstream, at distances greater than the width d of the channel.

The potential flow model does not account for the presence of the point air source, or the particular flux of gas. The shape of the slug is determined by the condition of constant pressure along the surface of the bubble. This is consistent with the experimental observation that the shape of the slug is independent of the gas flow rate. The length of the slug, on the contrary, is dependent on the gas flux: indeed, as the gas flux increases, the bubble length at the tail of the bubble also increases (figure 5).

4. Discussion

In this work we have described a series of new standing bubbles which can appear in a vertical pipe when air is added to a downward flux of water from the side of the pipe. We have shown that the dynamics of such bubbles is well described by classical potential flow theory. Also, as the gas flux supplied to the bubble decreases, the bubble becomes unstable and generates an oscillatory wake which carries a discrete flux of bubbles downstream, in a somewhat analogous fashion to the wake behind an obstruction in a confined channel.

Observation of these standing bubbles in a pipe with a downward liquid flow is of considerable interest for a number of reasons. First, from a theoretical perspective, these standing bubbles develop for a range of Froude numbers which are distinct from the case of a freely rising bubble. Second, the formation of a standing bubble leads to the shedding of a series of very small bubbles from its tail into the continuing flow; this may have importance for the formation of emulsions in two-phase flows within a pipeline. Thirdly, if the flow in the producing zone of a well encounters such standing slugs, the continuing flow past the slug will experience a substantial pressure loss and an intense zone of dissipation develops.

For the flow regimes analysed herein, the main cause of dissipation is the sudden expansion across the tail of the bubble. In this regard, we can use the momentum integral to estimate this decrease in pressure. If the area suddenly increases from A_1 to A_2 then the pressure jump as the flow expands is given by

$$\Delta p = \rho u_2^2\left(\frac{A_2}{A_1} - 1\right) \tag{5}$$

where subscripts 1 and 2 denote the properties upstream and downstream of the tail of the bubble.

In the present case, the liquid speed downstream of the bubble has value of order $1\,\mathrm{m\,s^{-1}}$, and the width of the liquid stream in the tail of the bubble, just above the point of breakup, is about 0.01 m. We therefore deduce that the pressure drop across the tail of the standing slug is of order 10^4 Pa. This is a significant pressure loss for the flow in comparison to the frictional pressure losses from the walls of the system. For example, with a drag coefficient of 0.01 on the walls of the system, and a length scale 0.1 m for the pipe diameter, the pressure loss per unit length of a pipe with a flow of speed $1\,\mathrm{m\,s^{-1}}$ is about $50\,\mathrm{Pa\,m^{-1}}$, so that the pressure loss in the expansion at the tail of the slug corresponds to the frictional losses along about 200 m of a pipe.

In closing, we note that there are many features of these bubbles for which it would be interesting to develop quantitative models. First, it would be valuable to study the relationship between the entrainment of gas from the tail of the standing bubbles and the liquid flow speed, since this might provide a key input to determine the length scale of the standing bubble; secondly, it would be interesting to explore the waves on the bubble surface, whose wavelength appears to increase with distance from the nozzle.

REFERENCES

Batchelor, G. K. 1967 *An Introduction to Fluid Dynamics*. Cambridge University Press.

Carberry, J., Sheridan, J. & Rockwell, D. 2005 Controlled oscillations of a cylinder: forces and wake modes. *J. Fluid Mech.* **538**, 31–69.

Clanet, C., Héraud, P. & Searby, G. 2004 On the motion of bubbles in vertical tubes of arbitrary cross-sections: some complements to the Dumitrescu–Taylor problem. *J. Fluid Mech.* **519**, 359–376.

Collins, R., De Moraes, F. F., Davidson, J. F. & Harrison, D. 1978 The motion of a large gas bubble rising through liquid flowing in a tube. *J. Fluid Mech.* **89**, 497–514.

Dake, L. P. 1979 *Fundamentals of Reservoir Engineering*. Elsevier.

Davies, R. M. & Taylor, G. I. 1950 The mechanics of large bubbles rising through extended liquids and through liquids in tube. *Proc. R. Soc. Lond.* A **200**, 375–390.

Deniz, S. & Staubli, Th. 1997 Oscillating rectangular and octagonal profiles: interaction of leading- and trailing-edge vortex formation. *J. Fluids Struct.* **11**, 3–31.

Dumitrescu, D. T. 1943 Ströming an einer luftblase im senkrechten rohr. *Z. Angew. Math. Mech.* **23**, 139–149.

Hiwada, M. & Mabuchi, I. 1981 Flow behaviour and heat transfer around the circular cylinder at high blockage ratios. *Heat Transfer Japan Res.* **10**, 17–39.

Keller, J. B. & Geer, J. 1973 Flow of thin streams with free boundaries. *J. Fluid Mech.* **59**, 417–432.

Rao, S. S. 1999 *The Finite Element Method in Engineering* 3rd edn. Butterworth-Heinemann.

Rhee, C. W., Talbot, L., Sethian, J. A. 1995 Dynamical behaviour of a premixed turbulent open V-flame. *J. Fluid Mech.* **300**, 87–115.

Richter, A. & Naudascher, E. 1976 Fluctuating forces on a rigid circular cylinder in confined flow. *J. Fluid Mech.* **78**, 561–576.

Roshko, A. 1954 On the drag and shedding frequency of two-dimensional bluff bodies. *NACA Tech. Note* 3169.

Vanden-Broeck, J. 1984*a* Bubbles rising in a tube and jets falling from a nozzle. *Phys. Fluids* **27** (5), 1090–1093.

Vanden-Broeck, J. 1984*b* Rising bubbles in a two-dimensional tube with surface tension. *Phys. Fluids* **27** (11), 2604–2607.

Vanden-Broeck, J. 1984*c* Numerical solutions for cavitating flow of a fluid with surface tension past a curved obstacle. *Phys. Fluids* **27** (11), 2601–2603.

Wegener, P. P. & Parlange, J. Y. 1973 Spherical cap bubbles. *Annu. Rev. Fluid Mech.* **5**, 79–100.